Janus MoSSe monolayer: superior and strain-sensitive gas sensing material

Cui Jin[1, 2], Xiao Tang[2], Xin Tan[3], Sean C. Smith[3], Ying Dai[1]*, Liangzhi Kou[2]*

[1]*School of Physics, State Key Laboratory of Crystal Materials, Shandong University, Jinan 250100, China*

[2]*School of Chemistry, Physics and Mechanical Engineering Faculty, Queensland University of Technology, Gardens Point Campus, QLD 4001, Brisbane, Australia*

[3]*Department of Applied Mathematics, Research School of Physics and Engineering, Australian National University, Canberra 2601, Australia*

daiy60@sina.com

Liangzhi.kou@qut.edu.au

Recent fabrication of Janus MoSSe monolayer has raised exciting prospects of the polar two-dimensional (2D) materials that exhibit excellent properties for nanodevice applications. Here, we proposed MoSSe as the superior gas sensing material by investigating the adsorption of CO, CO_2, NH_3, NO and NO_2 on the Janus layer by first-principles calculations. Due to the presence of out-plane polarization originated from the asymmetrical structure, it is found that NH_3 adopts distinct opposite orientations when it is adsorbed on Se or S side of the Janus layer. The binding strengths of all the molecules adsorption on Se surface are generally much stronger than these on the S surface. More interestingly, upon the strain deformation, the adsorption strengths of molecules NH_3 and NO_2 on Se side of MoSSe can be remarkably enhanced, but gradually lowered on S side. We revealed that the strain-dependent adsorption behavior is driven by a significant change of electrostatic potential difference between the Se and S surfaces under tensile strain. Corresponding to the distinct adsorption behaviors on two sides, different electronic variations are also revealed. With the higher gas selectivity, surface and strain selectivity, Janus MoSSe is proposed as an ideal material for constructing ultrahigh-sensitivity nanoscale sensors.

I. Introduction

Detecting gas molecules, especially toxic gases which induce the environmental pollutions, is important and critical to industry, agriculture and public health.[1] For example, the common gases like CO, CO_2, NH_3, NO and NO_2 are hazardous to the environment and can cause a number of health problems.[2] Thus, there is an increasing demand to develop highly sensitive, low cost and portable gas sensors with low power consumption. Electronic gas sensors based on the field effect transistors (FETs) can offer a simple, efficient but low-cost sensing platform for various chemical and biological detections.[3-6] Due to the inherent large surface-to-volume ratio, FETs gas sensor based on 2D layered nanomaterials is one of the most promising applications. For instance, graphene-based electronic sensors have been widely studied in the past few years. On the adsorption or desorption of molecules, the graphene-based sensors are actualized by monitoring the change in resistivity, which act as the charge acceptors or donors.[7-10] However, the intrinsic metallic feature of graphene limited the respond sensitivity of gas sensors.[11-14] Therefore, the 2D layered materials with semiconducting behavior is highly desired for a gas sensor with outstanding preformances. The semiconducting 2D layers with tunable electronic properties by the light or gate bias is particularly attractive since the transport characteristics can be modulated to enhance sensing performance.[15,16]

Due to the sizable band-gap and moderate carrier mobility, transition metal dichalcogenides (TMDs) have been demonstrated to be the idea 2D semiconducting materials for designing high sensitive FETs-based electronic gas sensors.[17-19] Experiments shown that the single and multi-layer MoS_2 film-based FETs are quite sensitive to a number of gas molecules, such as the CO, CO_2, NH_3 (5-50 ppm), NO and NO_2 (20 ppm), as indicated by changes of resistivity induced by adsorbed molecules that act as charge acceptors or donors.[20-23] The outstanding merits like high surface-to-volume ratio, selective reactivity upon exposure to a range of analytes, rapid response and recovery render MoS_2 a superior gas sensor with higher sensitivity and selectivity in comparison to graphene and other TMDs materials.[24-27] Espeicially, the sensing performance can be greatly enhanced since the band gap and the transport characteristics of MoS_2 are controllable with exposure to light or gate bias.[28-30] For instance, the selective chemical gas adsorption on monolayer MoS_2, and associated gas detection sensitivity, can be significantly modulated by the perpendicular applied electric field, as the electron transfer between gas molecules and MoS_2 can be tuned.[31]

However, it is still a big challenge to apply an external electric field and precisely control the adsorption behavior in the nanoscale. The material which possesses tunable intrinsic electric field to improve the sensitivities is highly desirable for ultra-high sensing performance. Recent synthesized Janus monolayer

MoSSe is one of the promising candidates. It was synthesized by fully replacing the S layers with Se atoms within MoS_2 at an applicable temperature mainly through the chemical vapor deposition (CVD) method.[32,33] Due to the mirror asymmetry, the Janus structure possesses an intrinsic out-of-plane dipole which induces large Rashba band splitting and out-of-plane piezoelectricity.[34-38] As a result, the photogenerated carrier can be separated in the photocatalyst reaction.[39-43] As the gas adsorption and sensing sensitivity can be enhanced by external electric fields in MoS_2,[31] it is expected that MoSSe possesses an enhanced gas sensing property, therefore it is highly desirable to explore and establish the trends and rules of gas molecule adsorption on the Janus MoSSe layer, and uncover the effects of interior electric field on the adsorption behaviors. To the best of our knowledge, no prior theoretical work has been conducted on these issues. It is expected that MoSSe will possess several advantages over MoS_2, such as the enhanced sensitivities induced by interior electric field and tunable selectivities originated from Janus strucutre, rendering it more suitable for ultra-sensitive gas sensor.

In this work, we examine the adsorption behaviors of several typical molecules CO, CO_2, NH_3, NO and NO_2 on MoSSe monolayer from first-principles calculations. It is found that, the interactions between these molecules and Janus MoSSe on the Se side are much stronger than that on the S side due to the presence of interior electric field. More interestingly, NH_3 presents the opposite adsorption orietations, different adsorption distances and strengths when it is adsorbed on the Se and S sides of the Janus layer. On application of uniaxial tensile strain, the adsorption strength of NH_3 and NO_2 adsorbed on Se side of Janus MoSSe further enhances, while that on the S side becomes weaker. The superior strain modulation can be explained by a significant change of electrostatic potential difference between the Se atom and S atom layers upon tensile strain. Correspondingly, the different adsorption behaviors of these gas molecules on both sides of Janus MoSSe lead to distinct electronic variations. The findings raised promising prospects of developing new Janus MoSSe-based ultrahigh-sensitivity nanodevices.

II. Computational methods

All the calculations are performed by means of the first-principles density functional theory (DFT),[44,45] as implemented in the Vienna Ab-initio Simulation Package (VASP),[46,47] within the framework of the projector augmented wave (PAW) method.[48] The generalized gradient approximation (GGA) with the Perdew-Burke-Ernzerhof (PBE)[49,50] functional is utilized to describe the exchange correlation interactions. In order to describe the van der Waals (vdW) interaction between gas molecules and MoSSe monolayer, we adopt the zero-damped DFT-D3 method proposed by Grimme.[51] In order to ensure the validity of our results, we also

calculated the gas adsorption on both sides of Janus MoSSe with other vdW correction methods (the DFT-D2 method of Grimme, and the DFT-D3 method with Becke-Jonson damping). The obtained results shown in Fig. S1, are very similar to these from zero-damped DFT-D3, indicating the method is applicable, we therefore based on the results from zero-damped DFT-D3 in the following. Spin polarization is employed in the calculations of the adsorption of NO and NO_2 since these molecules are paramagnetic, but not considered in the calculations for other gas molecules. A 4 × 4 supercell of monolayer MoSSe, with a single gas molecule adsorbed to it, is chosen as the computational model. Brillouin zone integration is sampled by a 5 × 5 × 1 k-grid mesh for geometry optimization, and 11 × 11 × 1 k-grid mesh for density of state calculations to achieve high accuracy. The vacuum space in the z-direction is set as large as 18 Å to avoid the interactions between the repeated slabs. A cutoff energy of 470 eV is chosen for the plane wave basis. Structure relaxations are carried out until the residual forces on atoms are less than 0.01 eV/Å. Convergence criterion of self-consistent calculations for ionic relaxations is set to 10^{-5} eV between two consecutive steps.

III. Results and discussion

Structurally, the Janus MoSSe monolayer is composed of a Mo atomic layer covalently bonded to Se atomic layer and S atomic layer (we will call them the Se-layer and S-layer in the following discussions) like a sandwich structure. Thus, the Mo atoms in the primitive cell are in six-fold coordination, while the S and Se atoms on the surfaces are in three-fold coordination. The corresponding lattice parameter of the unit cell is calculated as a = b = 3.25 Å, which is in good agreement with previous reports.[32-43] The lattice constant is between the values of MoS_2 (3.17 Å) and $MoSe_2$ (3.30 Å),[23,31,52-54] which is reasonable from the perspective of the composition of MoSSe. Then, we initially consider the adsorption geometries of CO, CO_2, NH_3, NO and NO_2 on both sides of Janus MoSSe. For each adsorption case, a gas molecule is placed on top of 4 × 4 surpercell of MoSSe layer, and the whole system is fully relaxed. Moreover, for each molecule, several possible adsorption sites and typical orientations have been considered, including the top site above the center of the hexagon, the top of the Mo (Se or S) atom and the top site above the Mo–Se (Mo–S) bond, the configurations with the molecule being parallel or perpendicular to the monolayer surface. The most favorable configurations for gas molecules adsorption on the Se-layer and S-layer of Janus MoSSe monolayer are presented in Fig. 1. For comparison purpose, we also determine the most stable structures for the adsorption of these molecules on MoS_2 and $MoSe_2$ monolayer, as shown in Fig. S2, which are well consistent with previous studies.[23,31,52-54] In the following, we will comprehensively investigate the gas sensing behaviors of MoSSe based on the adsorption distances, adsorption energies, electron transfer, surface potential variation and electronic variation, and compare with the corresponding values of MoS_2 and $MoSe_2$.

For CO adsorption (Fig. 1a and 1f), CO molecule is located at the bridge of the Mo–Se (Mo–S) bond next to one Mo atom on the Se-layer (S-layer), the distances are 3.23 and 3.15 Å, respectively. The C-O bond adopts tilted orientation with carbon atom pointing at the monolayer surface. In contrast, one of O atoms is located on top of Mo atom when CO_2 is adsorbed on top of MoSSe, two C-O bonds of CO_2 nearly parallel to the surface. The adsorption distance is 3.25 or 3.06 Å (Fig. 1b and 1g) on Se or S side. Since the two carbon-based gas molecules have innert chemical activities, the adsorption distances are more than 3 angstrom,which is in the range of weak van der Waals interactions. It is interesting to notice that the adsorption behavior on S (Se) layer of MoSSe is quite different from that on MoS_2 ($MoSe_2$) surface, implying the unique effects from the asymmetrical structures.

For the gas of NH_3, the adsorption behavior is distinct, as shown in Fig. 1c and 1h. The nitrogen atom in NH_3 sits at the center of the honeycomb, while hydrogen atoms point to the nearest three surrounding Mo atoms of the hexagonal ring, with an axis perpendicular to the monolayer surface. It is interesting to note that, NH_3 is bottom up adsorbed on S-layer where the N atom is away from the substrate, the direction of which is opposite to the cases on MoS_2 and $MoSe_2$ (Fig. S2). When it is adsorbed on Se side, NH_3 is bottom down with N atom close to Se-layer. The equlibrium distance at two sides are also slightly different, it is 2.71 Å when adsorbed on Se side, but 2.67 Å at S side. The phenomena is highly related with the polarization of NH_3 (direction is from H plane pointing to N plane) and the intrinsic dipole of Janus layer (pointing from Se-layer to S-layer), the superposition of two dipoles from NH_3 and MoSSe enhances the interior electric field on either side, therefore increasing the adsorption strengths like the example of external electric field enhanced gas sensing in MoS_2.[31] In Fig. 1d, 1e and 1i, 1j, the dipolar molecules NO and NO_2 prefer to locate in the hexagonal center near to the Mo atom on both layers. Similar to CO molecule, N-O bond of NO adopts a tilted orientation with nitrogen atom being closer to the monolayer surface, but the molecule NO_2 is perpendicular to the surface with oxygen atoms toward to the layer. The adsorption distance on the Se side is 2.82/2.84 Å while it is 2.77/2.78Å on the S side for these two gases. The adsorption configurations of NO and NO_2 on Janus MoSSe are nearly the same like these on monolayer MoS_2 and $MoSe_2$, seen in Fig. S2.

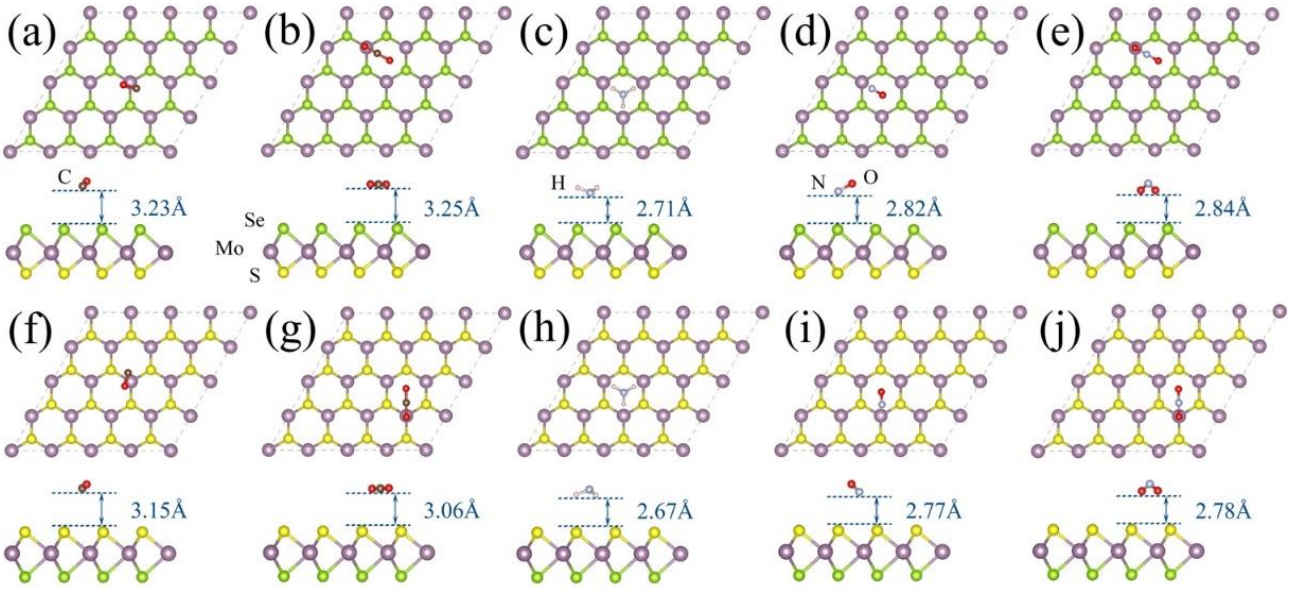

Fig. 1 Structural models and optimized structures of gas molecules CO, CO_2, NH_3, NO and NO_2 adsorption on the Se-layer (a-e) and S-layer (f-j). The atoms of monolayer and adsorbed molecules are denoted. The 4×4 super cell of Janus MoSSe monolayer is represented by the dashed lines. Purple, green and yellow balls are Mo, Se and S atoms respectively. Black, red, light grey and light pink represent C, O, N and H atoms respectively.

For a quantitative description of the adsorption behavior of molecules CO, CO_2, NH_3, NO and NO_2 on the Janus MoSSe, we summarized the equilibrium adsorption distances for all gases on both sides, as plotted in Fig. 2a. The corresponding distances for molecules adsorption on MoS_2 and $MoSe_2$ were also calculated in order to make a comprehensive comparison. One can see that the C-based gases have relative large adsorption distances, generally larger than 3Å, in the range of weak van der Waals interaction, belonging to physisorption. In contrast, the adsorption of NH_3, NO and NO_2 on Janus layer prefer chemical interactions with stronger binding strengths, which is in accord with the cases on monolayer MoS_2 and $MoSe_2$. When comparing the adsorption distances at two sides, it is interesting to find that equilibrium distance of all the studied molecules on Se-layer (black lines) is obviously larger than those on S-layer (red lines). In order to understand the interesting phenomena, we calculated the corresponding adsorption distances of these gases on MoS_2 and $MoSe_2$. The results show that such rule is absent, see dashed lines in Fig. 2a, the adsorption distance on $MoSe_2$ is not always larger than that on MoS_2. Especially, the adsorption distances for the gas CO (CO_2) on the MoS_2 and $MoSe_2$, as seen in Fig. S2, are 3.07 (3.14) and 3.08 (3.14) Å, respectively, there are basically no differences for CO (CO_2) adsorption on top of MoS_2 or $MoSe_2$. However, the adsorption distances of CO and CO_2 on two sides of Janus MoSSe are distinctly different, with the value difference around 0.08 to 0.19 angstrom, as seen

in Fig. 1. The contrast results clearly show that the different adsorption behaviors on the two sides have insignificant relationship with the dispersion forces of Se or S surface, but mainly from the interior electric field which is perpendicular to the Janus MoSSe plane structure (as discussed in the following).

The molecule-monolayer interaction strength is reflected by the adsorption energy of the gas molecules on different layers, we have calculated and plotted as the curves in Fig. 2b. Adsorption energy is defined as $E_a = E_{total} - E_{layer} - E_{gas}$, where E_{total} is the total energy of gas-adsorbed monolayer, and E_{layer} and E_{gas} are the energies of pristine monolayer (Se-layer, S-layer, MoS_2 and $MoSe_2$) and the isolated gas molecule (CO, CO_2, NH_3, NO and NO_2), respectively. A negative value of E_a indicates an exothermic adsorption. The more negative the E_a is, the stronger the gas is adsorbed. It is found that, the E_a values (magnitudes) of all the studied molecules adsorption on Se-layer are obviously larger than those on S-layer, indicating the surface selectivity of Janus MoSSe for these molecules. Therefore, gas molecules prefered to be adsorbed on the Se surface with higher binding strengths. In addition, among all the studied molecules, the E_a values (magnitudes) of NH_3 and NO_2 adsorption on Janus layer are obviously larger than others, leading to the higher selectivity to these molecules over C-based gases for MoSSe structure. Based on the findings it is expected that, NH_3 and NO_2 are more preferable to be adsorbed on the Janus layer with higher binding strengths in the environment where multiple gas species exist.

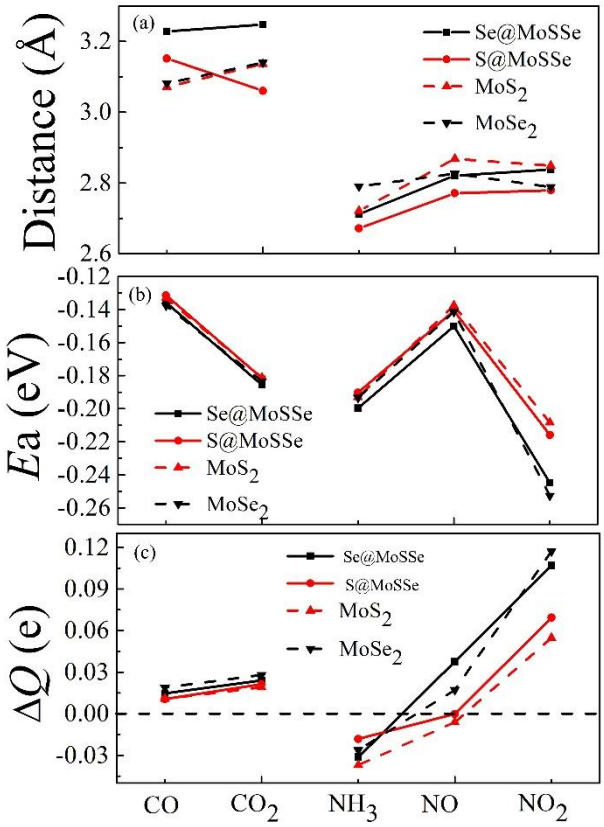

Fig. 2 The value of (a) adsorption distance d (Å), (b) adsorption energy E_a (eV), and (c) charge transfer ΔQ (e) of gas molecules CO, CO_2, NH_3, NO and NO_2 adsorption on Se-layer, S-layer, MoS_2 and $MoSe_2$,

respectively. The positive (negative) value of charge transfer represents gaining (losing) charge of the adsorbed gas molecule from (to) the layer.

Adsorption-induced charge transfer can induce the resistivity variation of the system, which is an important index to show the sensing merit and can be measured experimentally for gas sensors.[22,55] Fig. 3 presents charge density difference (CDD) images for molecule-monolayer systems, calculated by the formula $\Delta_\rho = \rho_{total} - \rho_{layer} - \rho_{gas}$, where ρ_{total}, ρ_{layer} and ρ_{gas} are the charge density of the gas-adsorbed MoSSe, pristine MoSSe, and isolated molecule (CO, CO_2, NH_3, NO and NO_2), respectively. Bader analysis is also performed to estimate the charge transfer value of gas molecules adsorption on different layers, as plotted in Fig. 2c and Fig. 3. The positive (negative) value of charge transfer represents gaining (losing) charge of the adsorbed gas molecules from (to) these layers. We find that charge redistribution of C-based gases adsorption on Se or S side of the monolayer is trivial, only a small amount of charges transfer from the layer to molecule, as shown in Fig. 3a-3b, accordingly causing relatively weak binding strength. For the N-based gas molecules, the significant charge redistribution of molecules and much more transfer amounts between adsorbates and MoSSe layers can be observed, indicating the higher sensitivity. There are several interesting phenomena worthy to be noticed. Firstly, CO, CO_2 and NO_2 on the MoSSe act as the charge acceptors but NH_3 molecule behaves as the charge donor to Se or S side of the monolayer, see Fig. 2c and Fig. 3c. Especially, NO acts as acceptor on Se side, but donator on S side (Fig. 3d) although the transferred electron amount is extremely small, the electron is remarkably redistributed in the NO gas molecule itself. Therefore the adsorption energy of NO on MoSSe is also quite small (Fig. 2b). Secondly, the significant charge transfer occurs on the case of NO_2 on Se side, which is up to 0.107e, it explained the strongest adsorption strength of molecule NO_2 adsorption on Se-layer. Thirdly, the amount of charge transfer of the adsorption of all studied molecules on Se-layer are much larger than the cases on S-layer, which explains the the findings in Fig. 2b, and also shows a clear correlation between the E_a and charge transfer, see Fig. 2b and 2c.

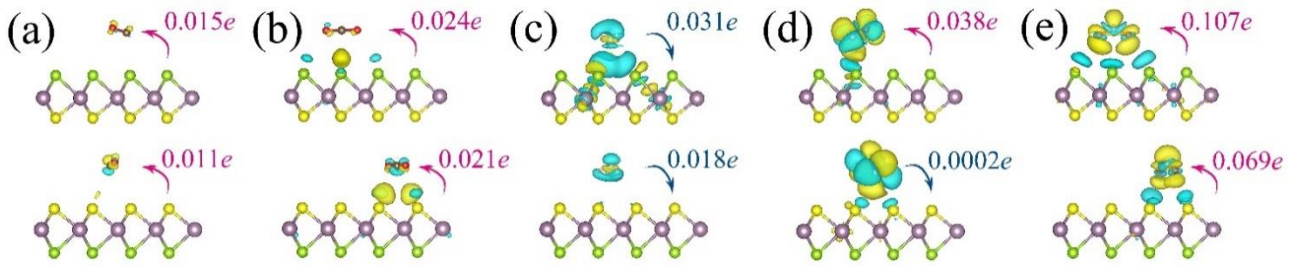

Fig. 3 Charge density difference (CDD) for gas molecules (a) CO, (b) CO_2, (c) NH_3, (d) NO, and (e) NO_2 adsorption on the Se-side (top panel) and S-side (bottom panel). The yellow (cyan) region represents charge

accumulation (depletion), and the isosurface value is 0.0003 e/Å^3. The orientation and value of charge transfer of these molecules adsorption on the Se and S surfaces are denoted.

As a result of gas adsorption, the electrostatic potential of MoSSe surface will be affected, which can lead to resistance change at the experimental measurements.[22,55] We present the variation of electrostatic potential of Se (S) surface of gas molecules (CO, CO_2, NH_3, NO and NO_2) adsorption on Se-layer (S-layer) in Fig. S3. Corresponding variations of potential values in comparison to pure MoSeS structure are summarized in the Table S1. It is found that, electrostatic potential values of adsorbed surface (Se or S) atoms are obviously moved up after gas adsoeption, with the magnutides of 0.01 to 0.16 eV, except for the adsorption of NH_3 on S side with decreased value of 0.06 eV.

In order to give a comprehensive picture of gas adsorption on the Janus materials, we also checked the adsorption behavior of oxygen on monolayer and NO_2 on bilayer system. The most favorable configurations for O_2 adsorption on both sides of Janus MoSSe are presented in Fig. S4. Corresponding adsorption distance, adsorption energy E_a and charge transfer are shown in the Tab. S2. The same as the considered gas above, binding strength and charge transfer amount of O_2 adsorption on Se surface are generally much larger than these on the S, confirming again the higher selectivity and sensitivity on the Se side than that on S side of Janus MoSSe. In addition, we also examined the adsorption behaviors on the bilayer MoSSe with NO_2 as the representative gas molecule, as seen in Fig. S5. Corresponding adsorption distance, E_a and charge transfer of NO_2 molecule adsorption on monolayer and bilayer MoSSe are summarized to Table S3. The same as monolayer, all the adsorption distance, adsorption energy and electron transfer on Se side are more obvious larger than that on the S side, which confirms again the higher selectivity and sensitivity on the Se side than S side on Janus layer. However, in comparison to the monolayer, there is a significant enhancement of E_a (magnitudes) and charge transfer amount of NO_2 molecule adsorption on both sides of bilayer MoSSe, which imply that bilayer Janus MoSSe is probably more suitable for ultra-sensitive gas sensors.

We also examine the adsorption of gas molecules on both sides of Janus MoSSe upon uniaxial tensile strain (from 1% to 5%). The strain is defined as $\varepsilon = (a - a_0)/a_0$, where a_0 and a are the lattice parameters of the unit cell without strain and with applied strain, respectively. For simplicity, NH_3 and NO_2 molecules are chosen as the representative N-based gas molecules to study in this discussion while CO_2 is chosen as an example of C-based gas. Fig. 4 illustrates the strain modulation of the adsorption distance and E_a with the applied uniaxial tensile strain on gas-adsorbed monolayer. Our calculations indicate that the adsorption of NH_3 and NO_2 on both Se and S sides of the monolayer are highly sensitive to the strain conditions, but exhibiting the different

dependences on the opposite sides. For example, the adsorption distances of NH_3 on both sides are increased by the strain. However, the E_a values of NH_3 adsorption on Se-layer decrease linearly with the rising strain, whereas these on S-layer increase, see Fig. 4b. For NO_2 adsorption, the distance to the Se side is increased linearly while that to S side is decreased. The adsorption strength is enhanced (weakened) at Se (S) side, see Fig. 4d. It means that, the application of uniaxial tensile strain (within 5%) leads to a further enhanced adsorption strength for NH_3 and NO_2 on Se-layer, but a gradual lowering of the adsorption strength on S-layer. Thus, Se-layer (S-layer) of Janus monolayer MoSSe exhibits enhanced (decreased) sensitivity toward the adsorption of NH_3 and NO_2 after applying uniaxial tensile strain, which demonstrates the strain selectivity for gas adsorbed MoSSe monolayer. Based on the findings, a strain dependent gas sensor can be proposed where the NH_3 and NO_2 molecules can be captured or released by varying the tensile strains in Janus MoSSe layer in a practical environment. These conclusions are still valid under the biaxial strain, although the variations of adsorption distance and strength by biaxial tensile strain are more significant (Fig. S6). The adsorption of CO_2 on both sides of Janus MoSSe upon uniaxial tensile strain (from 1% to 5%) are shown in Fig. S7. In contrast to the opposite variations of N-based gas molecule, the adsorption strengths for CO_2 molecule are enhanced on both Se and S sides with the application of tensile strain, probably due to the different polarization of the molecules.

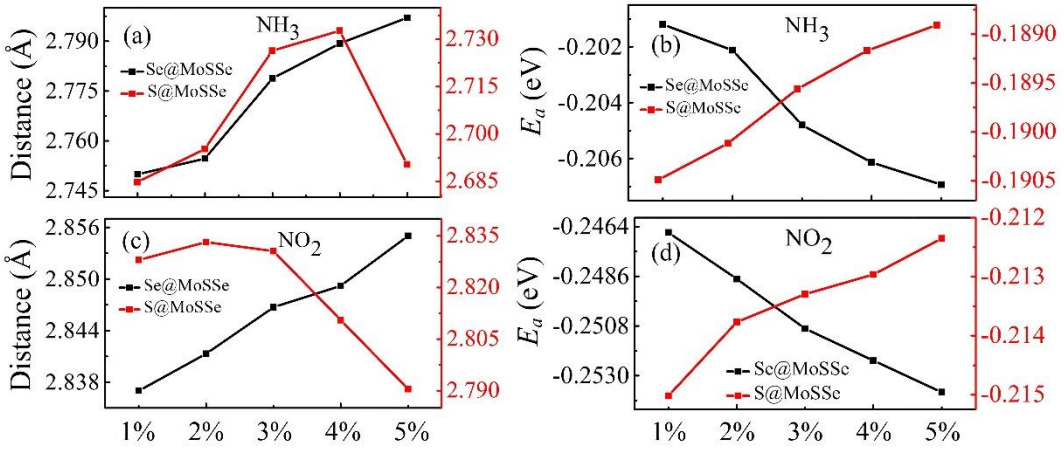

Fig. 4 Top panel: the variation of (a) adsorption distance d (Å), and (b) adsorption energy E_a (eV) of the gas molecule NH_3 adsorption on Se-layer and S-layer, respectively, as the function of applied uniaxial tensile strain. Bottom panel: the variation of (c) adsorption distance d (Å), and (d) adsorption energy E_a (eV) of the gas molecule NO_2 adsorption on Se-layer and S-layer, respectively, as the function of applied uniaxial tensile strain.

To analyze the underlying physical mechanism for the strain-dependent behavior, we calculate the planar

average of the electrostatic potential of pristine MoSSe without and with the applied tensile strain. It is known that there is no electrostatic potential difference between two S atomic layers for the pristine MoS_2 because of the same element on both sides of monolayer. On the contrary, the Se atomic layer possesses a larger electrostatic potential value than S layer on MoSSe structure, which leads to an interior electric field across the out-plane direction. From the calculations of work function, we can see an electrostatic potential difference of $\Delta\Phi$ = 2.47 eV between Se and S surfaces, as seen in Fig. 5, in accord with previous calculations.[39] The electric field can be approximately estimated as 0.76 V/Å (the thickness of MoSSe is 3.25 Å). The adsorption of the gas molecules on the Se (S) side can be regarded as these adsorbed on $MoSe_2$ (MoS_2) under external electric field of 0.76 V/Å.[31] It is therefore easy to understand the enhanced selectivity and different sensing behavior in the new MoSSe monolayer as discussed above. Interestingly, it is found that the potential difference ($\Delta\Phi$) between Se and S surfaces is tunable which is decreasing from 2.47 eV to 2.31 eV by applying uniaxial tensile strain of 5%. As a result, the built-in electric field in MoSSe can be regulated by strain deformation, which help to adjust the selectivity and sensitivity toward the adsorption of molecules. This also reasonably explained the strained-induced variation of adsorption behavior in Fig. 4. It's worthy to point out although the gas sensing property of MoS_2 is also tunable under strain deformation,[23] it is originated from bonding environment change rather than the variation of interior electric field in Janus MoSSe. The findings here therefore unveal a new mechanism for strain modulated gas sensitivity.

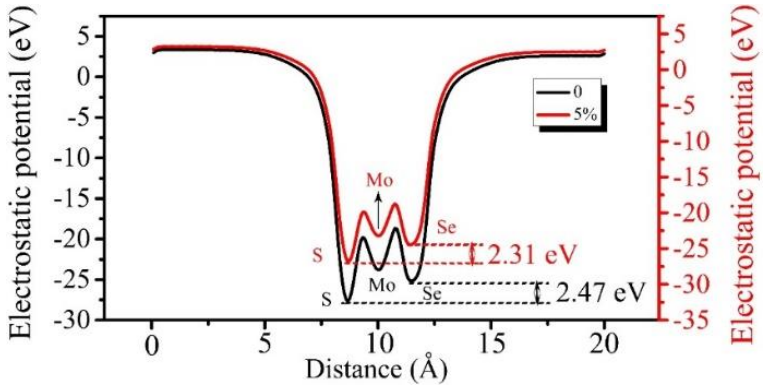

Fig. 5 The planar average of the electrostatic potential of pristine MoSSe without (the line of black colour) and with the applied uniaxial tensile strain of 5% (the line of red colour). Electrostatic potential difference $\Delta\Phi$ (eV) between Se and S atomic layers without and with strain are denoted, respectively.

From the experimental measurements, adsorption-induced resistance variation is measured to check the sensitivity for gas sensors.[22,55] Resistance variation can be mainly reflected by the binding energy, electron

transfer, and electronic variations from theoretical calculations.[23,31] We now turn to the effects of gas adsorption on the electronic properties of Janus MoSSe. The total density of states (TDOS) of Janus MoSSe with the adsorption of CO, CO_2, NH_3, NO and NO_2 molecules are shown in Fig. 6, as well as the projected DOS from the gas molecules. The results show a band gap of 1.54 eV for pristine MoSSe, as seen in Fig. 6a, in accordance with previous PBE results of the gap value in MoSSe structure.[32,33] It is well-known that standard PBE calculations usually underestimate the band gap of semiconductors, but it is reliable to predict for trends.[55] We find that the TDOS for either the valence or conduction band of MoSSe is not significantly influenced upon the molecules CO and CO_2 adsorption, which is consistent with their weak van der Waals adsorption, see Fig. 6b and 6c. The energy states from CO or CO_2 are located at the deep energy level around 4 eV below or above the Fermi level, see insets of Fig. 6b and 6c. However, we can still see the state differences for the gases on Se or S side, both the CBM and VBM are relatively shifted (the insets, red and black lines) due to the presence of interior electric field as indicated above. In the case of NH_3, as shown in Fig. 6d, there are noticeable downward shifting of the valence and conduction band edges for NH_3 adsorption on the S-layer in comparison to that on the Se-layer as a result of interior electric field and polarization of gas molecule. The conclusion is also confirmed by aligning the potential energy of band edges, namely taking the vacuum level as a standard. For other two magnetic molecules NO and NO_2, the adsorption on MoSSe will induce the asymmetric magnetic states into the band gap, see Fig. 6e and 6f, still we can see the difference when NO or NO_2 is adsorbed on Se and S sides. For example, a new spin state is induced near the Fermi level when NO is on Se side, but it is absent when on S side. The new spin state for NO2 adsorbed on Se surface is located at 0.3 eV, but it is at 0.8 eV above the Fermi level when the gas molecule on the oppsite surface. The revealed electronic difference and distinct adsorption behavior on Se or S side of MoSSe imply the possibilities to design new and superior gas sensors based on the Janus MoSSe layer.

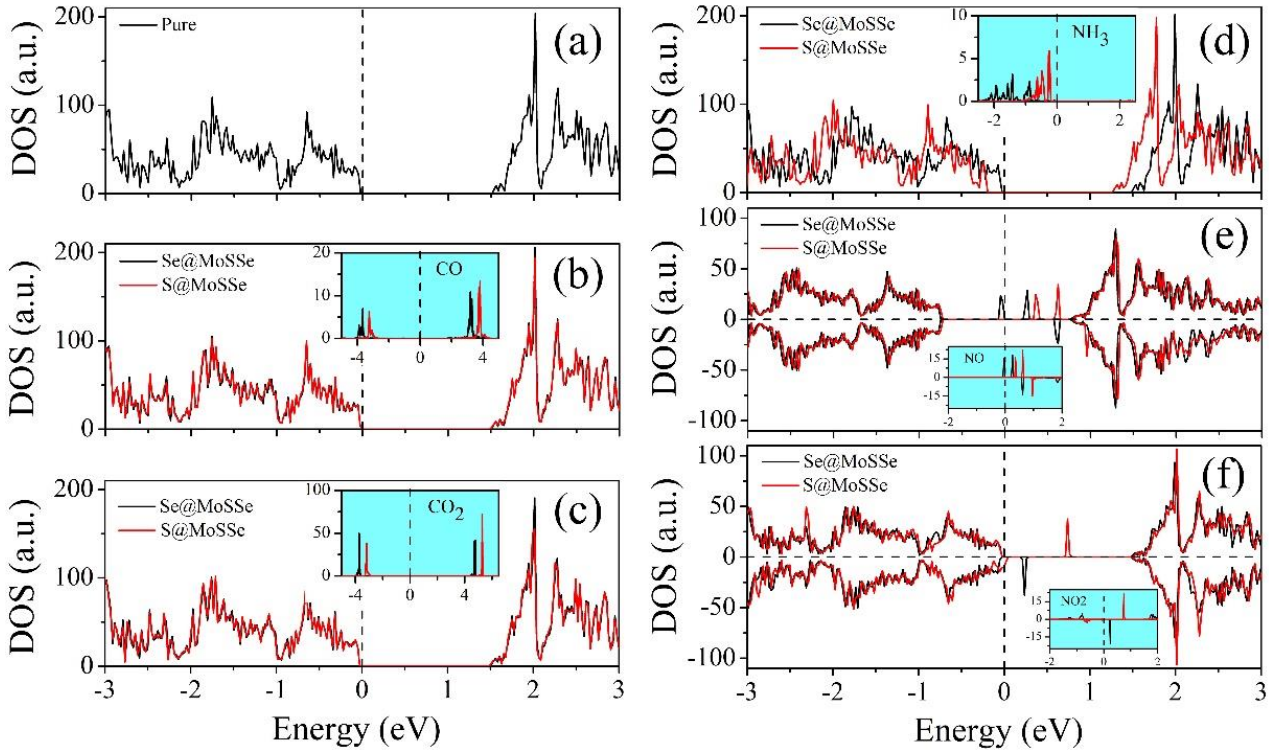

Fig. 6 Calculated total density of states (TDOS) of the (a) pristine MoSSe, gas molecules (b) CO, (c) CO_2, (d) NH_3, (e) NO, and (f) NO_2 adsorbed Se-layer and S-layer, respectively, with the PBE method. The insets show the projected DOS from these gas molecules. The black (red) lines represent gas molecules adsorption on the Se-layer (S-layer). The Fermi level is set to zero.

IV. Conclusions

In conclusion, we theoretically estimate the gas sensing performance of Janus MoSSe monolayer for CO, CO_2, NH_3, NO and NO_2 adsorption. Our results predict that the adsorption of N-based gases on MoSSe are chemical interactions and the adsorption of C-based gases belong to physisorption. Among all the gas molecules, NH_3 presents the distinct opposite orientations between the adsorption on Se and S atom sides of the monolayer. Note that, binding strengths of the molecules adsorption on Se-layer are much stronger than the cases on the S-layer, facilitating the adsorption (desorption) of gases on (from) the Se (S) atom side of the monolayer MoSSe. On the other hand, application of uniaxial tensile strain (within 5%) leads to further enhanced (gradual lowering) adsorption strengths for NH_3 and NO_2 on Se-layer (S-layer). Therefore, the NH_3 and NO_2 molecules can be captured or released by varying the applied tensile strains in Janus MoSSe layer. The strain-dependent adsorption behavior is driven by a marked change (0.16 eV) in electrostatic potential difference between Se and S surfaces of monolayer MoSSe upon tensile strain. Notably, the electronic properties of MoSSe can be modulated upon the gas adsorption depending on different adsorption behaviors on Se and S atom sides of

Janus MoSSe. With the intrinsic built-in electric field, Janus MoSSe is thus demonstrated as the idea gas sensing material due to the enhanced gas sensitivity, surface selectivity and strain selectivity. The results obtained in this work shed light on the exciting prospects of developing Janus MoSSe-based ultrahigh-sensitivity gas sensing nanodevices.

Acknowledgements

We acknowledge generous grants of high-performance computer time from the computing facility at Queensland University of Technology and Australian National Facility. C. J. gratefully acknowledges financial support by China Scholarship Council (CSC, 201706220175). L. K. gratefully acknowledges financial support by the ARC Discovery Early Career Researcher Award (DE150101854).

References

1. J. Kong, N. R. Franklin, C. Zhou, M. G. Chapline, S. Peng, K. Cho and H. Dai, *Science*, 2000, **287**, 622-625.
2. X. Chen, C. K. Y. Wong, C. A. Yuan and G. Zhang, *Sens. Actuators, B,* 2013, **177**, 178-195.
3. Y. L. Guo, G. Yu and Y. Q. Liu, *Adv. Mater.*, 2010, **22**, 4427-4447.
4. P. A. Hu, J. Zhang, L. Li, Z. L. Wang, W. O'Neill and P. Estrela, *Sensors*, 2010, **10**, 5133-5159.
5. X. Song, J. Hu and H. Zeng, *J. Mater. Chem. C*, 2013, **1**, 2952-2969.
6. X. Chen, C. Tan, Q. Yang, R. Meng, Q. Liang, M. Cai, S. Zhang and J. Jiang, *J. Phys. Chem. C*, 2016, **120**, 13987-13994.
7. F. Schedin, A. K. Geim, S. V. Morozov, E. W. Hill, P. Blake, M. I. Katsnelson and K. S. Novoselov, *Nat. Mater.*, 2007, **6**, 652-655.
8. O. Leenaerts, B. Partoens and F. M. Peeters, *Phys. Rev. B*, 2008, **77**, 125416.
9. T. O. Wehling, K. S. Novoselov, S. V. Morozov, E. E. Vdovin, M. I. Katsnelson, A. K. Geim and A. I. Lichtenstein, *Nano Lett.*, 2008, **8**, 173-177.
10. D. Yang, N. Yang, J. Ni, J. Xiao, J. Jiang, Q. Liang, T. Ren and X. Chen, *Mater. Des.*, 2017, **119**, 397-405.
11. Z. Sljivancanin, F. Besenbacher, B. Hammer, T. G. Pedersen, P. Hofmann and L. Hornekaer, *Nat. Mater.*, 2010, **9**, 315.
12. I. Meric, M. Y. Han, A. F. Young, B. Ozyilmaz, P. Kim and K. L. Shepard, *Nat. Nanotechnol.*, 2008, **3**, 654.

13. Q. Tang, Z. Zhou and Z. Chen, *Nanoscale*, 2013, **5**, 4541-4583.
14. R. Meng, X. Lu, S. Ingebrandt and X. Chen, *Adv. Mater. Interfaces*, 2017, **4**, 1700647.
15. G. Korotcenkov, *Mater. Sci. Eng. B*, 2007, **139**, 1-23.
16. J. Pang, Q. Yang, X. Ma, L. Wang, C. Tan, D. Xiong, H. Ye and X. Chen, *Phys. Chem. Chem. Phys.*, 2017, **19**, 30852-30860.
17. X. Tang, A. Du and L. Kou, *WIREs Comput. Mol. Sci.*, 2018, **8**, e1361.
18. A. Kuc, T. Heine and A. Kis, *MRS Bull.*, 2015, **40**, 577-584.
19. L. Zhou, L. Kou, Y. Sun, C. Felser, F. Hu, G. Shan, S. C. Smith, B. Yan and T. Frauenheim, *Nano Lett.*, 2015, **15**, 7867-7872.
20. Q. He, Z. Zeng, Z. Yin, H. Li, S. Wu, X. Huang and H. Zhang, *Small*, 2012, **8**, 2994-2999.
21. H. Li, Z. Yin, Q. He, H. Li, X. Huang, G. Lu, D. W. H. Fam, A. I. Y. Tok, Q. Zhang and H. Zhang, *Small*, 2012, **8**, 63-67.
22. B. Cho, M. G. Hahm, M. Choi, J. Yoon, A. R. Kim, Y. J. Lee, S. G. Park, J. D. Kwon, C. S. Kim, M. Song and Y. Jeong, *Sci. Rep.*, 2015, **5**, 8052.
23. L. Kou, A. Du, C. Chen and T. Frauenheim, *Nanoscale*, 2014, **6**, 5156-5161.
24. Y. Huang, J. Guo, Y. Kang, Y. Ai and C. M. Li, *Nanoscale*, 2015, **7**, 19358-19376.
25. T. Xie, G. Xie, Y. Su, D. Hongfei, Z. Ye and Y. Jiang, *Nanotechnol.*, 2016, **27**, 065502.
26. C. N. Rao, K. Gopalakrishnan and U. Maitra, *ACS Appl. Mater. Interfaces*, 2015, **7**, 7809-7832.
27. P. F. Liu, L. Zhou, T. Frauenheimc and L. M. Wu, *Nanoscale*, 2016, **8**, 4915-4921.
28. D. J. Late, Y. K. Huang, B. Liu, J. Acharya, S. N. Shirodkar, J. Luo, A. Yan, D. Charles, U. V. Waghmare, V. P. Dravid and C. N. Rao, *ACS Nano*, 2013, **7**, 4879-4891.
29. A. Kuc and T. Heine, *Chem. Soc. Rev.*, 2015, **44**, 2603-2614.
30. N. Zibouche, P. Philipsen, T. Heine and A. Kuc, *Phys. Chem. Chem. Phys.*, 2014, **16**, 11251-11255.
31. Q. Yue, Z. Shao, S. Chang and J. Li, *Nanoscale Res. Lett.*, 2013, **8**, 425.
32. A. Y. Lu, H. Zhu, J. Xiao, C. P. Chuu, Y. Han, M. H. Chiu, C. C. Cheng, C. W. Yang, K. H. Wei, Y. Yang, Y. Wang, D. Sokaras, D. Nordlund, P. Yang, D. A. Muller, M. Y. Chou, X. Zhang and L. J. Li, *Nat. Nanotechnol.*, 2017, **12**, 744-749.
33. J. Zhang, S. Jia, I. Kholmanov, L. Dong, D. Er and W. Chen, *ACS Nano*, 2017, **11**, 8192-8198.
34. L. Dong, J. Lou and V. B. Shenoy, *ACS Nano*, 2017, **11**, 8242-8248.
35. Y. Guo, S. Zhou, Y. Bai and J. Zhao, *Appl. Phys. Lett.*, 2017, **110**, 163102.
36. R. Peng, Y. Ma, S. Zhang, B. Huang and Y. Dai, *J. Phys. Chem. Lett.*, 2018, **9**, 3612-3617.

37. Y. Ma, L. Kou, B. Huang, Y. Dai and T. Heine, *Phys. Rev. B*, 2018, **98**, 085420.
38. X. Tang, S. Li, Y. Ma, A. Du, T. Liao, Y. Gu and L. Kou, *J. Phys. Chem. C*, 2018, **122**, 19153-19160.
39. X. Ma, X. Wu, H. Wang and Y. Wang, *J. Mater. Chem. A*, 2018, **6**, 2295-2301.
40. Z. Guan, S. Ni and S. Hu, *J. Phys. Chem. C*, 2018, **122**, 6209-6216.
41. Y. Ji, M. Yang, H. Lin, T. Hou, L. Wang, Y. Li and S. T. Lee, *J. Phys. Chem. C*, 2018, **122**, 3123-3129.
42. H. Jin, T. Wang, Z. R. Gong, C. Long and Y. Dai, *Nanoscale*, 2018, **10**, 19310-19315.
43. Y. Liang, J. Li, H. Jin, B. Huang and Y. Dai, *J. Phys. Chem. Lett.*, 2018, **9**, 2797-2802.
44. P. Hohenberg and W. Kohn, *Phys. Rev.*, 1964, **136**, B864.
45. W. Kohn and L. J. Sham, *Phys. Rev.*, 1965, **140**, A1133.
46. G. Kresse and J. Furthmüller, *Phys. Rev. B*, 1996, **54**, 11169.
47. G. Kresse and D. Joubert, *Phys. Rev. B*, 1999, **59**, 1758.
48. P. E. Blöchl, *Phys. Rev. B*, 1994, **50**, 17953.
49. J. P. Perdew and Y. Wang, *Phys. Rev. B*, 1992, **45**, 13244.
50. S. Grimme, *J. Comput. Chem.*, 2006, **27**, 1787-1799.
51. S. Grimme, J. Antony, S. Ehrlich and H. Krieg, *J. Chem. Phys.*, 2010, **132**, 154104.
52. M. Sharma, P. Jamdagni, A. Kumar and P. K. Ahluwalia, *AIP Conf. Proc.*, 2016, **1731**, 140045.
53. D. J. Late, T. Doneux and M. Bougouma, *Appl. Phys. Lett.*, 2014, **105**, 233103.
54. J. Baek, D. Yin, N. Liu, I. Omkaram, C. Jung, H. Im, S. Hong, S. M. Kim, Y. K. Hong, J. Hur, Y. Yoon and S. Kim, *Nano Res.*, 2017, **10**, 1861-1871.
55. L. Kou, T. Frauenheim and C. Chen, *J. Phys. Chem. Lett.*, 2014, **5**, 2675-2681.